Soft Scissor: A Cartilage-inspired, Pneumatic Artificial Muscle for Wearable Devices

Nahian Rahman[1], Richard Suphapol Diteesawat[1], Sam Hoh[1], Leah Morris[2],
Ailie Turton[2], Mary Cramp[2], Jonathan Rossiter[1]

Abstract—Although rigid exoskeletons can strengthen human capabilities or provide full assistance to patients with disabilities, their rigidity may constrain natural movement, developing tissue damage in long-term usage. Soft and semi-soft exoskeletons and exosuits exhibit both compliance and comfort, and offer the potential to provide practical and widely-adopted assistance. Soft pneumatic muscles have been explored as a means to drive wearable assist devices for over a decade; however, their softness leads to compromises in terms of power output and the precision by which forces can be applied to the human body. In this article, we introduce a novel soft extending pneumatic actuator, which combines a compliant scissor structure inspired by human cartilage and soft pneumatic muscles. The structure behaves as a compliant skeleton to the force generating pneumatic muscle, guiding its actuation behaviour and maintaining high force transmission through its body. Different designs and dimensions of the actuator and structure were investigated to observe the effect of compliance on key performance parameters. A soft single-module actuator can deliver extending force over 100 N and achieve a maximum strain of 178% when inflated at 50 kPa. A slightly thicker, but still compliant, continuum two-module actuator exhibits twice the extension compared to a single-module actuator with the same design under the same load up to 4 kg, a significant and suitable force for comfortable wearable devices. Last, a wearable prototype of this novel actuator is demonstrated, exhibiting both extension and bending actuation behaviours.

Index Terms—Soft Robot Materials and Design, Soft Robot Applications, Wearable Robotics, Actuation and Joint Mechanisms

fig. 1. A continuum three-module cartilage-inspired pneumatic actuator designed as a prototype for a wearable device: (a) front and top views and (b) being held aside a human knee. Its actuation modalities include (c) extension and (d) extension plus bending.

I. INTRODUCTION

THERE is a worldwide trend of ageing populations, as global life expectancy rises and birth rates decline. According to the United Nations [1], the number of older persons worldwide is expected to double over the next three

decades. As older persons are more likely to suffer from neuro-musculoskeletal disabilities that result in lower mobility [2], this trend highlights a growing need for advancements in assistive devices and rehabilitation treatments. Robotic technologies have been identified as a prime candidate for revolutionising these fields, as they hold great promise for returning patients to independent and productive lives and for supplementing rehabilitative training and exercise [3]. Although rigid exoskeletons [4], [5] provide significant assistance and reduce physiotherapists' workload [6], concerns regarding patient's safety remain such as joint misalignment, difficulties in donning/doffing, weight and appearance, adaptability, and cost.

The exploration of soft, wearable powered devices for use in rehabilitative and assistive applications has been of particular interest in the recent decade, resulting in various prototypes [7]–[9] and even a commercially available product, the ReStore exosuit [10]. Such technologies are particularly

attractive as long-term assistive devices because they are significantly lighter. Their compliance allows them to conform and adapt to a wearer, making them more comfortable and reducing the incidence of injuries [11] that arise from poor alignment; a problem that is common with some rigid devices [12], [13]. However, the benefit of comfort and adaptability also comes at a cost: an increase in compliance results in less effective force transmission, meaning that softer wearable devices cannot be used to provide the full assistance necessary for nonambulatory individuals to return to normal walking [8]. This is in comparison to fully rigid exoskeletons such as ReWalk [14] and Ekso [15], which are designed to provide full support to individuals with spinal cord injury.

Pneumatic artificial muscles (PAMs), elastomers, and fabric-based actuators have been widely explored by the research community in the soft wearable robotics field [16], [17]. In general, they inherit lightweight, compliance and flexibility and offer high tensile force upon pressurization with high force-to-weight ratio. Origami rigid or semi-rigid structures have been integrated to improve the actuation performance of either positive-pressure extending actuators [18], [19] or negative-pressure contracting actuators [20].

In this paper, we introduce a novel continuum pneumatic actuator for future wearable assist devices (a prototype is shown in fig. 1), which combines a soft scissor structure, inspired by human cartilage, and a flexible fabric with integrated pneumatic chambers. In nature, cartilage is stiffer and less flexible than muscle, but is less rigid than bone. It fulfils many important roles including providing shape and structure to parts of the body (e.g. the ears), acts as a cushion or shock absorber (e.g. in the knee) and can be an anchor for muscles (e.g. in the nose). These characteristics make cartilage, and cartilage-like materials and structures very attractive for future soft assistive and rehabilitative devices. We present the concept and design of this new cartilage-inspired actuator and investigate the effect of compliance of the soft structure on the actuator performance.

II. Materials and Methods

A. Concept and Design

The developed pneumatic actuator (fig. 1) combines a soft scissor structure made from cartilage-inspired materials and a pneumatic chamber. The cartilaginous scissor structure is used as a compliant skeleton to guide actuation direction and force transmission, while the integrated pneumatic chamber behaves as a muscle, enabling extension actuation when it is inflated (fig. 2). The scissor structure can be created as an arbitrary-sized continuum structure by building several modules in series, as exemplified by the two-module structure in fig. 2(b) and the three-module knee actuator in fig. 1.

Each module of a scissor structure consists of four links made of soft rectangular blocks of the cartilage-inspired material with soft joints connecting each block as shown in fig. 2(a). The width, length, and height of each block and joint are defined as w_b, l_b, h_b, w_j, l_j, and h_j, respectively. For a scissor structure with more than one module, two connecting
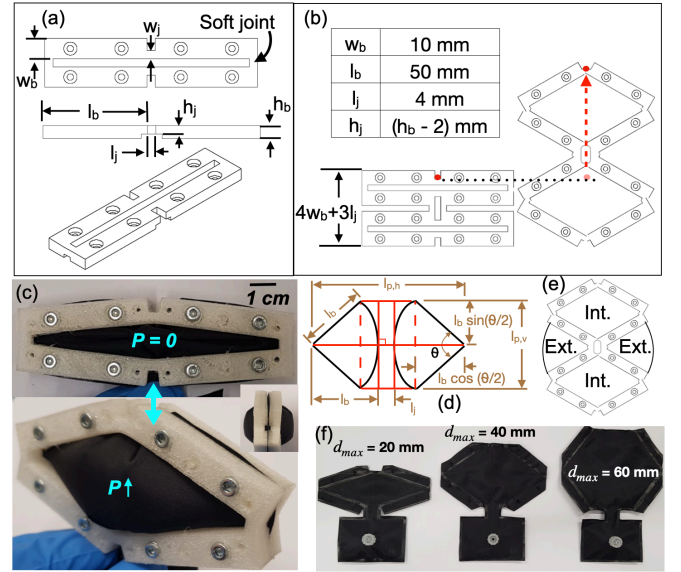
fig. 2. (a-b) Schematic diagram of (a) a one-module scissor structure in top, front and isometric views, including design parameters, and (b) a two-module scissor structure in rest and actuated states. Inset table shows the values used in this study. (c) The fabricated pneumatic actuator combining a one-module scissor structure and a pneumatic chamber in rest state with no pressure and in a pressurised state. (d) Design parameters of a flat fabric used to make the pneumatic chamber, (e) position of internal and external pneumatic chambers on a scissor structure, and (f) a range of fabricated chambers for a one-module scissor structure.

joints with the same dimension (w_j, l_j and h_j) are added between adjacent modules (fig. 2(b)). The scissor structure is fabricated using a compliant material in order to deliver an entirely soft pneumatic actuator. However, different levels of compliance can affect actuation behavior and performance; softer materials give flexibility to the structure, enabling safe human interaction, but limit the level of assistance provided. The effect of compliance was investigated by varying the joint and block dimensions of the scissor structure.

The hexagonal pneumatic chamber was designed to form two identical end-to-end cones at maximum inflation, with the cones connected at their bases in the middle of the actuator as shown in fig. 2(c). This shape was defined by two parameters: a targeted vertical extending length at maximum inflation (d_{max}) at the middle of the actuator, and the slant height of the cones, which is equal to the block length, l_b. The pneumatic chamber is fabricated by heat-sealing two pieces of identical, inextensible flat fabric.

To achieve this double-cone shape from a flat fabric, the deflated shape is formed by unwrapping the slanted surface of the cone and placing half of the flattened cone surface on one side of the fabric as shown in fig. 2(d). This design is defined by l_b, and the arc length is half of the circumference of the cone base, equal to $\frac{\pi}{2} d_{max}$. The centres and apexes of the cones are aligned along the x axis and their orientations are mirrored. The ends of the arcs of each cone are connected together to simplify fabrication, creating a hexagon as the final shape of the deflated chamber. An additional length equal to the joint length (l_j) is added between their arcs in the x axis

so that the horizontal length of pneumatic chamber is equal to the total length of a scissor structure at a built shape ($2l_b + l_j$). Hence, the horizontal and vertical lengths of the fabric needed to fabricate a pneumatic chamber ($l_{p,h}$ and $l_{p,v}$) can be derived using the following equations. In addition, the angle θ can be calculated from $\frac{\pi}{2} \cdot \frac{d_{max}}{l_b}$.

$$l_{p,h} = 2l_b + l_j \quad \text{and} \quad l_{p,v} = 2l_b \cdot \sin(\frac{\pi}{4l_b} \cdot d_{max}) \quad (1)$$

B. Fabrication

The cartilage-inspired scissor structure is fabricated from flexible TPU (NinjaFlex TPU filament, NinjaFlex, USA) which has a tensile strength of 12 MPa, approximately in the middle range of human articular cartilage (5-25 MPa) [21]. It was printed in a single build using a 3D printer (FlashForge Creator Pro 2, FlashForge, UK) with 60% infill density. The block width and length (w_b and l_b) and joint length (l_j) are fixed for all investigations at 10, 50 and 4 mm, respectively, as shown in fig. 2(b). The block height (h_b) is varied for different experiments, but the joint height (h_j) is fixed at 2 mm less than h_b for all h_b.

A pneumatic chamber was made of TPU-coated nylon fabric (Riverseal® 70 LW, Rivertex, UK) and fabricated using a heat sealer (HS400C, Polybags, UK). An air tube connector was made of a luer adapter (45518-82, Cole-Parmer, UK), M6 nylon nut (528-148, RS, UK) and nitrile rubber O-rings (0066-24, RS, UK). The scissor structure was designed to contain two holes on each block to which the pneumatic chamber could be mounted, as shown in fig. 2(c). Hence, a complete cartilage-inspired pneumatic actuator can be made by sandwiching the fabric pneumatic chamber between two identical scissor structures and clamping the structure together with short bolts and nuts. The integrated pneumatic chamber within the scissor structure is referred to as the internal pneumatic chamber. This internal chamber naturally folds within the scissor structure at no actuation. For actuators with more than one module, external pneumatic chambers are added to both the left and right sides of the scissor structures as shown in fig. 2(e). These external chambers provide additional support and improve the actuation performance.

C. Experimental setup

Two testing rigs were used for mechanical experiments. A horizontal experimental setup (fig. 3(a)) was used for force-strain evaluation of the scissor structures as well as isobaric and isometric tests to evaluate the performance of one-module and two-module pneumatic actuators. A vertical experimental setup (fig. 3(b)) was used for isotonic testing to evaluate the extension behaviour of the pneumatic actuators at various loads.

The horizontal setup (fig. 3(a)) consisted of a 3D-printed attachment to mount the scissor structures or pneumatic actuators to the moving platform of a linear actuator (500 mm C-beam linear actuator, Ooznest, UK), which was used to control extension. The extension was obtained by measuring the displacement of the attachment using a laser displacement sensor (LK-G402, Keyence, UK). The other end of the scissor
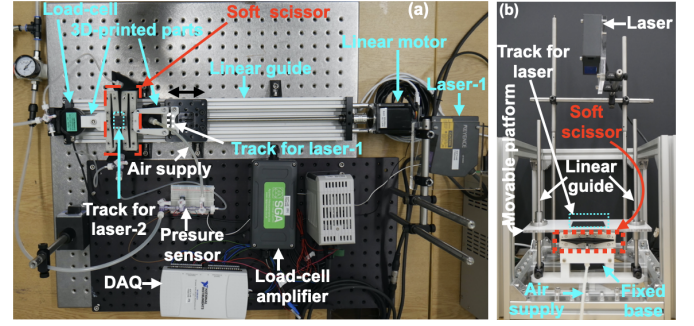
fig. 3. Experimental setup for (a) force-strain, isobaric and isometric tests (top view), and (b) isotonic test (front view).

structure was attached to a 100 N S-beam load cell (DBCR-100N-002-00, Applied Measurements Ltd., UK) for measuring both the restoring forces of the cartilaginous scissor structures and blocking forces of pneumatic actuators.

For force-strain evaluation, prior to each experiment, scissor structures (with no pneumatic chambers) were initially set at their built length (l_{built}). The l_{built} of a one-module scissor structure is $2w_b + l_j$, and thus l_{built} = 24 mm for all one-module structures (fig. 2(a)). The experiments were performed by continuously extending the structures at a speed of 0.25 mm/s using the linear actuator, while the force and extension were measured. The extension is then reported in the results as strain (ε), which is defined as the percentage ratio of the displacement of the attachment to l_{built}. Several structures made of different joint shapes and joint width (w_j) were studied in this force-strain experiment to assess their stiffness in the axial direction.

Isobaric experiments were performed to evaluate blocking force generation of one-module pneumatic actuators when actuated at different pressures. The actuators were inflated using an air compressor (P100/24 AL, Werther International S.p.A., Germany) and the pressure was controlled and recorded using a pressure regulator and a pressure sensor (HSC-DANN030PGAA5, Honeywell International Inc.). One actuator end was attached to the moving platform on the linear actuator while the other end was pressed against an attachment connected to the load cell. The experiments were started at l_{built}, and a constant air pressure was applied, generating a force against the load cell. The moving platform of the linear actuator was then moved away from the load cell. The linear actuator was stopped when force was no longer detected, corresponding to the instant when the actuator detached itself from the load cell.

Isometric experiments were performed with the horizontal test setup and two-module pneumatic actuators to investigate the effects of structure compliance on actuation performance. One end of the actuator was attached to the 3D-printed attachment on the linear actuator while the other end was free from the load cell. Prior to each experiment, the linear actuator was set at a specific extension between 10 and 50 mm, where zero displacement is l_{built}. During the experiments, the internal pneumatic chamber pressure (P_{int}) was increased from 0 to 50 kPa while force was recorded. Note that, for any extension, the internal pressure must rise to a pressure

where the actuator first makes contact with the load cell, and blocking force can be recorded. To evaluate the support provided by the external chambers, the same experiments were repeated by also actuating both sides of the external pneumatic chambers, which were inflated and maintained at constant pressure (P_{ext}). The vertical (out-of-plane) displacement at the central connecting joint between two modules was observed by an additional laser sensor (LG-402, Keyence, Japan) marked as *track for laser-2* in fig. 3(a). All two-module actuator experiments were stopped when either P_{int} reached 50 kPa or the vertical displacement of the connecting joint exceeded 10 mm.

The vertical setup was built to perform isotonic (gravimetric) tests. The actuators were mounted vertically to the base of the frame and to a vertical free-moving platform (fig. 3(b)). Different loads were added to the top of the platform, and the actuators were slowly inflated from 0 to 50 kPa within 10 seconds, by manually controlling the pressure regulator, while vertical extension was measured by a laser displacement sensor pointed at the platform.

All experiments were operated through MATLAB (The MathWorks Inc.), and the data was recorded using a data acquisition device (USB-6211, National Instruments, USA). Each experiment was performed three times, and the resultant data are presented as mean and standard deviation.

III. RESULTS

A. Restoring force of scissor structure

Unlike a free-rotating rigid hinge, the soft joints in the scissor structure generate a restoring force when the structure is pulled or stressed. This restoring force defines the level of intrinsic structural compliance, as it is related to the structure's stiffness. Therefore, compliance of the scissor structures was investigated by varying joint shape and dimension. Three different joint shape profiles were tested: a rectangular shape, a rectangular shape with one side curved and a rectangular shape with both sides curved (shapes are shown in the inset of fig. 4), where h_b is fixed at 6 mm. In addition to the difference in joint shape profiles, two different values of w_j at 2 and 4 mm were used to build six scissor structures in total. During the experiments, they were pulled from 0 to 60 mm extension, corresponding to a strain between 0 and 250% when l_{built} = 24 mm.

Figure 4 illustrates that the restoring force for different joint shapes is similar; however, significant difference occurs when varying w_j. An increment in w_j from 2 to 4 mm results in 3.5 times larger restoring force. The restoring force of all structures increases linearly up to 150% strain in a repeatable manner. As the both-side curved joint at w_j = 2 mm contains the least amount of material of all joints, it offers the lowest stiffness. In contrast, the rectangular joint with w_j = 4 mm delivers the highest restoring force with smaller variance due to the highest material volume in its joints. We observed that the rectangular joints provide predictable outcome in repeatable manner. Therefore, it is used in latter experiments.
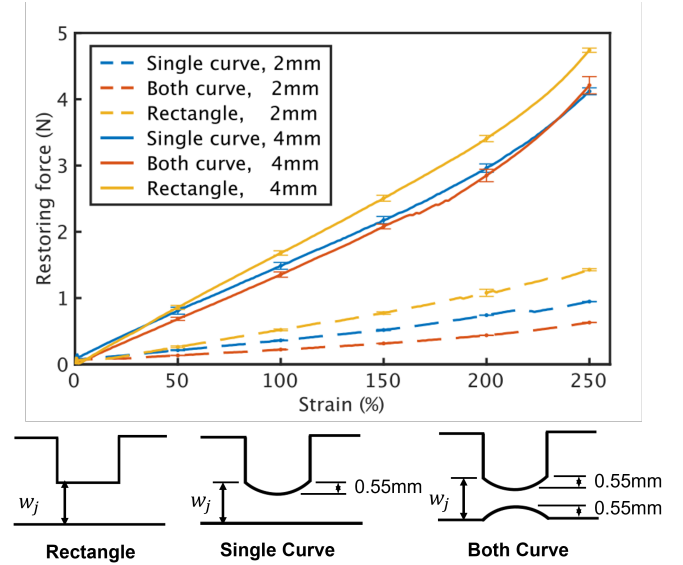
fig. 4. Force-strain evaluation of six one-module scissor structures with different joint shapes and widths. Lower diagram shows the different joint profiles.

B. Isobaric experiments on one-module actuators

Isobaric experiments were performed to evaluate the performance of three one-module pneumatic actuators made with different pneumatic chambers (d_{max} = 20, 40 and 60 mm) but the same scissor structure (w_j = 2 mm and h_b = 6 mm). Each actuator was inflated at a constant pressure of 10, 30 and 50 kPa. Figure 5 shows isobaric actuation of these three actuators at different pressures. The blocking forces of all actuators increased with increasing pressure at the same extending strain, and larger pneumatic chambers delivered better actuation performance in both force and extension. Despite different pressure actuation, similar maximum strains were achieved, and the mean value of their maximum strain across different pressures are 45%, 112%, and 178% for the pneumatic chambers with d_{max} = 20, 40 and 60 mm, respectively. Actuation comparison between these actuators can be seen in the Supplemental Movie.

The force profiles of the actuator with d_{max} = 60 mm are slightly different at low strain when actuated at the pressure of 10 and 30 kPa (fig. 5(c)). This behaviour is due to folding of the larger pneumatic chamber within the scissor structure when in the initial state; the chamber could only fully unfold when the linear actuator moved up to a certain extension, after which extension behaviour matched the general trend of the other chambers. This behaviour disappeared at 50 kPa as the pressure was sufficient to unfold the fabric in the initial state.

Figure 6(a) compares the behavior of these three actuators made of different pneumatic chamber geometries at 50 kPa. Their force-strain profiles are almost parallel, which provides a large predictable operating span for use in many applications. In addition, a pneumatic actuator made of a scissor structure with w_j of 4 mm and a pneumatic chamber with d_{max} = 40 mm was tested for three pressures (10, 30 and 50 kPa), to demonstrate the effect of increasing w_j. Its actuation result is included in fig 5(b) (in red), and its extending force follows a
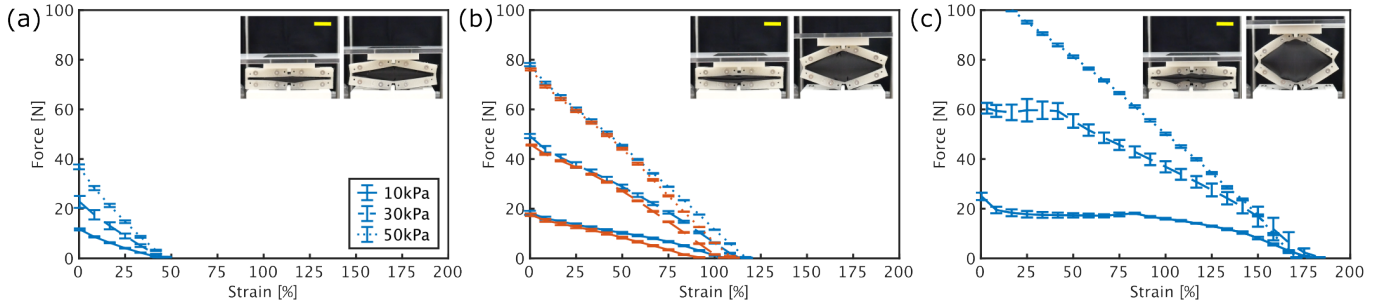
fig. 5. Isobaric evaluation of three one-module pneumatic actuators made with fixed scissor dimensions of w_j = 2 mm and h_b = 6 mm but different pneumatic chambers (d_{max}) of (a) 20 mm, (b) 40 mm, and (c) 60 mm. All actuators were pressurised at 10, 30 and 50 kPa. Insets show images of the actuators at rest and at 50 kPa, where yellow bars indicate 2 cm length. The profile of the actuator made of w_j = 4 mm, h_b = 6 mm and d_{max} = 40 mm is included in (b), in red, to compare the effect of different w_j.

similar pattern to the actuator with the structure made of w_j = 2 mm. As expected, the actuator with w_j = 4 mm shows a slight decrease in generating force due to the increase in intrinsic restoring force, which implies higher stiffness in the axial direction following the finding in fig. 4.

Figure 6(b) describes the effect of increasing thickness of the scissor structure (h_b = 6, 9, and 12 mm but the same w_j = 4 mm) on the force-strain performance at different pressures. The increase in structure thickness naturally leads to an increase in stiffness. It is observed that at higher pressures, actuators made of a thicker structure provide greater force although they exhibit the same trend in their force-strain profiles at different pressures. This behaviour could be because the thicker material (h_b) increases the contact area between the scissor structure and the pneumatic chamber at lower extensions (approximately between 0 and 15 mm), which allows higher force transmission to the structure. This contact area occurs for all pneumatic chambers at low extension and reduces with increasing extension. Different d_{max} varies this area at a given extension; lower d_{max} causes a smaller area, and different h_b will show little to insignificant benefit for small d_{max}.

C. Isometric experiments on two-module actuators

In this experiment, three two-module continuum actuators were built using scissor structures made of rectangular joints with w_j = 4 mm but different h_b of 6, 9 and 12 mm, of which their weight is 67, 77 and 122 gm, respectively. The l_{built} of all two-module actuators are the same at 52 mm. The internal pneumatic chamber was fabricated using d_{max} = 40 mm. External pneumatic chambers at both sides of the scissor structure were designed to match half of the internal chamber with d_{max} = 40 mm. As described in experimental setup, these actuators were fixed at constant extension between 10 and 50 mm and the pressure of external chamber (P_{ext}) was fixed at 0, 10 and 30 kPa prior to all experiments. The internal pneumatic chamber was inflated from 0 to 50 kPa (P_{int}). Since the two-module actuator has an additional compliance in the connecting joints, vertical (out-of-plane) displacement was observed at a certain pressure while the actuator was constrained horizontally. Therefore, we set the experiments to
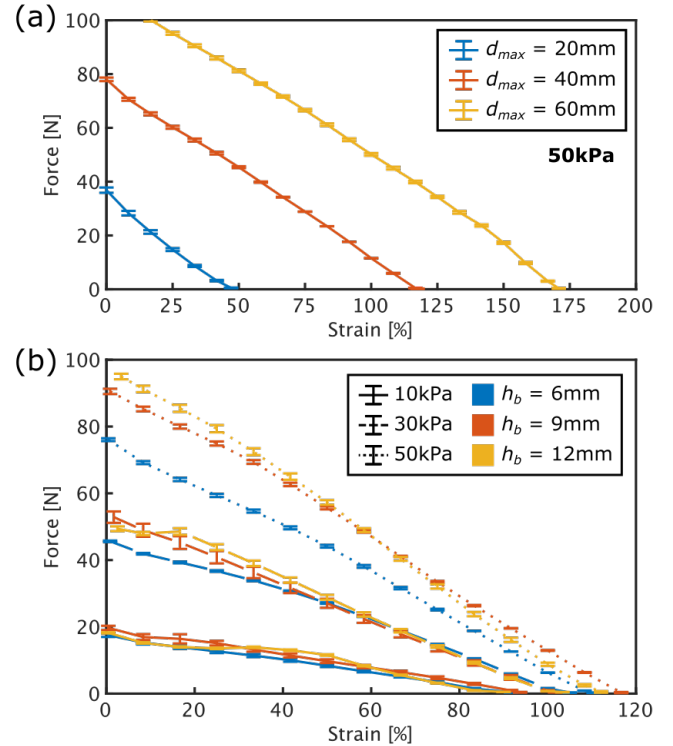
fig. 6. Comparison of the force-strain relationship between different one-module pneumatic actuators made of (a) a rectangular joint of w_j = 2 mm and and h_b = 6 mm but different pneumatic chambers at 50 kPa and (b) the same rectangular joint of w_j = 4 mm and pneumatic chambers (d_{max}) of 40 mm but different structure thickness, h_b, of 6, 9 and 12 mm.

stop when either P_{int} reached 50 kPa or 10 mm of vertical displacement was reached.

Figure 7(a) shows the force-pressure relationship of the two-module continuum actuator with h_b = 9 mm. At fixed extension of 10, 20 and 30 mm, the experiments were stopped since the vertical displacement limit was reached, while the remaining experiments were stopped when the pressure reached 50 kPa. Experimental results were converted to force-strain relationships at various P_{int} (fig. 7(b)). The maximum generated force (F_{max}) obtained at different strains up to a vertical displacement of 10 mm or actuated pressure of 50 kPa is included.
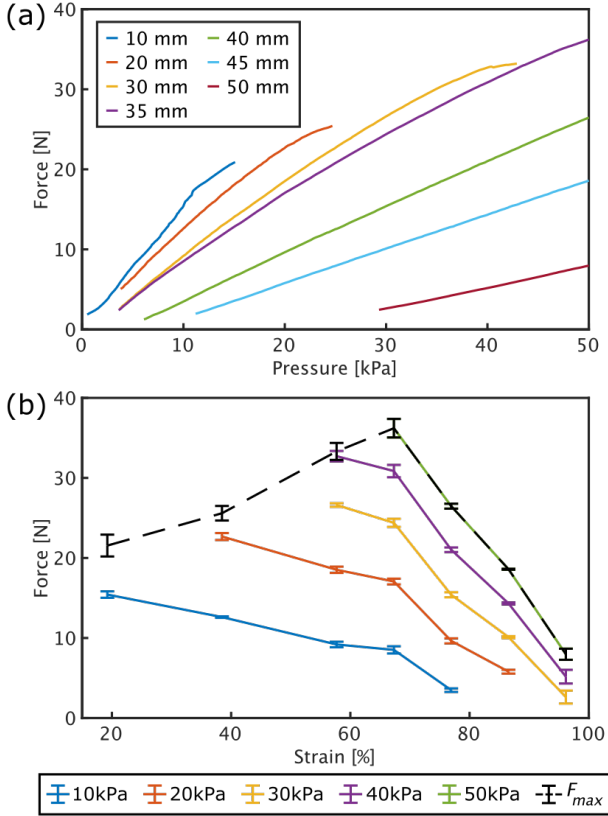
fig. 7. Isometric force evaluation of the two-series-module, scissor-inspired pneumatic actuators when actuating only an internal pneumatic chamber at operating pressures between 0 and 50 kPa, showing the relationship between (a) force and pressure and (b) force and extension. The maximum forces (F_{max}) obtained at different extensions are shown as a dashed line.

The same experiments were conducted for actuators with h_b = 6 and 12 mm to investigate the effect of structure stiffness (higher thickness implies higher stiffness). F_{max} and pressure at F_{max} at different strains of all three actuators are presented in fig. 8, where solid, dashed and dotted lines indicate the actuation of external pneumatic chambers at 0, 10 and 30 kPa, respectively. Reinforcing the structures with pressurised external chambers improved their actuation performance regardless of structure thickness, increasing maximum force generation (fig. 8a). The pressure of the internal pneumatic chamber at which F_{max} was achieved at different strains is shown in fig. 8(b). As the strain increased, the achievable internal pressure within the 10 mm vertical displacement limit rose.

Comparing the performance of these actuators shows an improvement of force transmission with an increase in structure thickness or stiffness. The stiffer structure showed reduced vertical displacement either with or without reinforcement from external pneumatic chambers, enabling them to achieve higher F_{max} and internal pressure at F_{max}. In particular for the stiffest structure (h_b = 12 mm), its vertical displacement never reached the 10 mm threshold, allowing the actuator to always be inflated up to 50 kPa (fig. 8(b)). Despite the minor force reduction for this thicker structure at larger strains, it exhibited the highest F_{max} of 87 N, occurring at P_{int} = 50

kPa and P_{ext} = 30 kPa. The force pattern of the thicker (h_b = 12 mm) two-module actuator behaves similar to a one-module pneumatic actuator made of the same structure design (yellow dotted line in fig. 6(b)). In contrast, the two thinner continuum actuators (h_b = 6 or 9 mm) are influenced by their compliance, and out-of-plane displacement reduces the maximum force they can generate.

Overall, when increasing w_j the restoring force increases (fig. 4), and this effect decreases the generated strain of the pneumatic actuator (fig. 5(b)). This implies increasing stiffness in axial direction. On the other hand, increasing h_b reduces off-plane deformation and improves axial force transmission from the inflated pneumatic chambers through the compliant scissor structure (fig. 8). We can conclude that increasing joint dimension in a selected axis increases the structure stiffness in that axis, for instance, joint width (w_j) for axial stiffness and joint thickness (h_b) for off-plane stiffness.
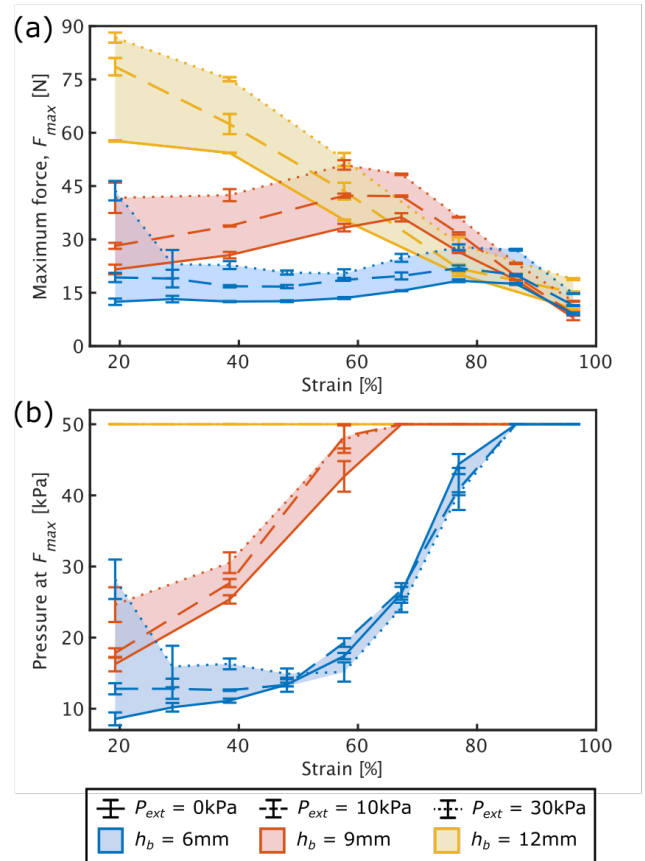
fig. 8. (a) Maximum force generation (F_{max}) and (b) pressure at F_{max} of the internal pneumatic chamber of three two-module actuators made of different structure thickness, h_b = 6, 9 and 12 mm, shown as blue, red and yellow lines, respectively. Actuation of external pneumatic chambers at different pressures, P_{ext} = 0, 10 and 30 kPa, are defined as solid, dashed and dotted lines. Coloured areas highlight the actuation of the same pneumatic actuator.

D. Isotonic experiments

Isotonic test was conducted for the pneumatic actuators with both one-module and two-module scissor structures made of the same w_j = 4 mm and h_b = 9 mm. Different constant loads between 0 and 4 kg (including the 0.2 kg platform) were

undertaken. In these experiments, the pressure was regulated up to 50 kPa while the platform position was monitored by a laser sensor. Figure 9(a) and 9(c) report the recorded displacement and pressure at different loads for the one-module actuator and two-module actuator, respectively. For the two-module actuator, both internal and external pneumatic chambers were connected and inflated at the same pressure.

It can be seen that the slopes of these plots are greater initially and reduce as the pressure rises. In addition, it is observed that with an increasing load, the initial displacement goes below zero at 0 kPa as a result of structure compression. This is due to the natural gap in the designed structure where the pneumatic chambers are placed (one module: l_j, two module: $3l_j$, see fig. 2(b)). This negative displacement is eliminated after a certain pressure in a repeatable manner. Nevertheless, this can be eliminated easily by using the displacement as feedback for a pressure control algorithm or simply by adding a mechanical end stop. We observe that the standard deviation increases for certain loads (for example 3.2 kg in fig. 9(a) and 4.2 kg in fig. 9(c)). These variances occur due to either the unfold behaviour or the structure compliance, which alter actuator behaviour at high loading as the platform rises. This will be explored in future work. Example actuation of these actuators at 0.2 kg and 4.2 kg loads can be seen in the Supplemental Movie.

IV. CONCLUSION

In this work, a new soft pneumatic artificial muscle is presented, which was reinforced by a cartilage-inspired scissor structure. This soft structure was used as a compliant skeleton to constrain the actuation behaviour of internal pneumatic chambers, resulting in an extending actuator. Using these materials, the actuator is fully soft and flexible when not actuated, benefiting safe interaction and ease of wearing. The performance of one-module and two-modules pneumatic actuators made of different dimension scissor structures and pneumatic chambers were investigated.

For one-module actuators, higher pressure improves the actuation performance of all actuators, and larger pneumatic chambers increase both force generation and maximum strain because of higher contact surface between the chamber and the scissor structure, increasing force transmission through the structure (fig. 5). The maximum force over 100 N and the strain of 178% were delivered at 50 kPa by a soft actuator with the largest pneumatic chamber (d_{max} = 60 mm). This maximum force is 340 times its own weight (30 gm), corresponding to the specific force of 3.33 N/g at 50 kPa. This is in the range of other positive-pressure actuators: woven or knitted fabric-based actuators (approx. 15-50 N at 50 kPa, [16]) and origami-based bellow-like actuators (1 kg or 1.18 N/g at 24 kPa, [18]).

This suggests that the design and size of pneumatic chambers can be optimized to achieve better performance in the future work. The force-strain profiles across different one-module actuators inflated at the same pressure follow the same trend, independent of the size of the pneumatic chambers or thickness of scissor structures (fig. 6).

(a)

(b)

(c)

(d)
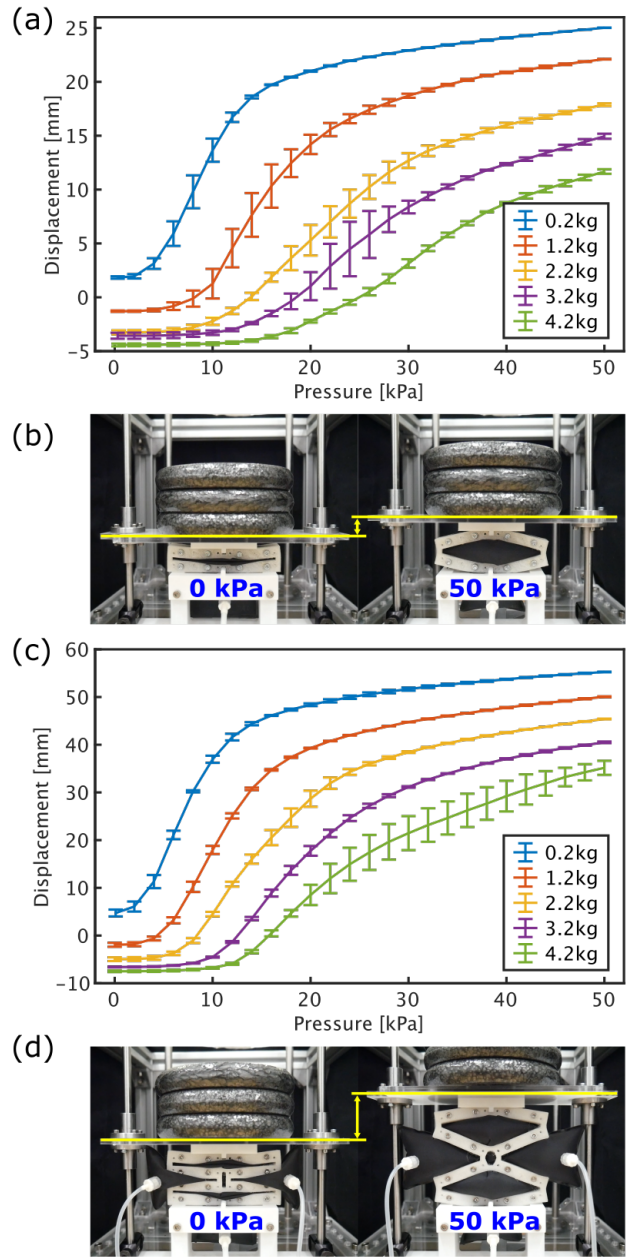
fig. 9. The results of isotonic experiments showing the relationship between displacement and pressure of (a) one-module and (c) two-module pneumatic actuators while lifting different constant loads. The dimension of the scissor structures and pneumatic chambers are identical (w_j = 4 mm, h_b = 9 mm and d_{max} = 40 mm). Actuation of (b) one-module and (d) two-module actuators at 50kPa while lifting 4kg weight. Yellow lines indicate the height of the platform.

The effect of compliance on actuator performance can be observed in continuum pneumatic actuators when varying the thickness of scissor structure, which implies different intrinsic stiffness of the actuators (fig. 7 and 8). As a result, the stiffest two-module actuator (h_b = 12 mm) exhibits actuator behaviour similar to the one-module actuator shown in fig. 6(b) as it can be inflated up to targeted pressure, delivering the maximum force of 87 N (at P_{int} = 50 kPa and P_{ext} = 30 kPa). In contrast, higher out-of-plane deflection was detected in softer two-module continuum actuators, limiting the max-

imum force generation and achievable pressure; for example, approximately 15 N and 30 N for actuators made with $h_b = 6$ and 9 mm, respectively. However, with reinforcement provided by the external pneumatic chambers, the performance of all actuators were improved.

The comparison of isotonic actuation between one-module and two-module actuators made of the same dimension of scissor structure ($w_j = 4$ mm, $h_b = 9$ mm) and pneumatic chamber ($d_{max} = 40$ mm) was also investigated (fig. 9). This demonstrates that the 77 gm continuum actuator reinforced by external pneumatic chambers can deliver approximately twice the extension as a single-module actuator under the load up to 4.2 kg (55 times its own weight) (fig. 8(a)) which indicates practical scaling of these structures to larger arrays. The continuum actuator reached its maximum extension within 3 seconds, corresponding to the inflation speed of 18.33 mm/s or 11.66 mm/s while lifting only 0.2 gm platform or 4.2 kg load, respectively. This is dependent on the supplied air flow from a compressor or pump.

Moreover, different actuation combinations between internal and external pneumatic chambers can result in various expanded shapes and motions, especially extending and bending. By varying block length (l_b in fig. 2) between left and right sides of consecutive modules, it is possible to mimic bending motion, for example, patient-specific knee joint motion. Designing external pneumatic chambers with larger size than the internal chamber and scissor structure can also improve bending motion. Besides, the scissor design of this cartilage frame can be exploited as an endoskeleton for negative pressurization as [20]. These concepts will be explored as the next investigation. The actuator fabrication is facile, by simply sandwiching the pneumatic chambers between the cartilage structures, and each component is easy to fabricate. The pneumatic chambers can be flexibly designed to deliver a desired strain (d_{max}). However, if the pneumatic chamber becomes larger than the scissor frame when inflated (fig. 2(c)), this may result in unwanted interactions. This can potentially be solved by developing a new fabrication and design to create a 3D pneumatic chamber, whereby its inflated size does not exceed the structure.

Finally, the concept of this novel pneumatic actuator was used to create a compliant, lightweight, three-module prototype with the weight of 117 gm as a potential wearable device shown in fig. 1. The scissor structure was designed to have a curved shape to conform to human limbs. When actuating all pneumatic chambers, the actuator extends in the axial direction, whereas actuating only one side of external chambers with an internal chamber allows extending and bending motions (see Supplemental Movie). Force transmission and motion range of this potential prototype will be evaluated in future work to prove the effectiveness in assisting human mobilities. In addition, we aim to develop a dynamic simulator for the scissor structure to build an optimal, patient-specific knee device that can mimic and assist their natural movement.

REFERENCES

[1] U. N. D. of Economic and P. D. Social Affairs, "World population ageing 2020 highlights: Living arrangements of older persons."

[2] A. Freemont and J. Hoyland, "Morphology, mechanisms and pathology of musculoskeletal ageing," *The Journal of Pathology: A Journal of the Pathological Society of Great Britain and Ireland*, vol. 211, no. 2, pp. 252–259, 2007.

[3] R. Gassert and V. Dietz, "Rehabilitation robots for the treatment of sensorimotor deficits: a neurophysiological perspective," *Journal of neuroengineering and rehabilitation*, vol. 15, no. 1, pp. 1–15, 2018.

[4] H. Zhu, C. Nesler, N. Divekar, V. Peddinti, and R. Gregg, "Design principles for compact, backdrivable actuation in partial-assist powered knee orthoses," *IEEE/ASME Transactions on Mechatronics*, 2021.

[5] J. Wang, X. Li, T.-H. Huang, S. Yu, Y. Li, T. Chen, A. Carriero, M. Oh-Park, and H. Su, "Comfort-centered design of a lightweight and backdrivable knee exoskeleton," *IEEE Robotics and Automation Letters*, vol. 3, no. 4, pp. 4265–4272, 2018.

[6] E. Read, C. Woolsey, C. A. McGibbon, and C. O'Connell, "Physiotherapists' experiences using the ekso bionic exoskeleton with patients in a neurological rehabilitation hospital: A qualitative study," *Rehabilitation Research and Practice*, vol. 2020, 2020.

[7] H. K. Yap, J. H. Lim, F. Nasrallah, and C.-H. Yeow, "Design and preliminary feasibility study of a soft robotic glove for hand function assistance in stroke survivors," *Frontiers in neuroscience*, vol. 11, p. 547, 2017.

[8] A. T. Asbeck, S. M. De Rossi, K. G. Holt, and C. J. Walsh, "A biologically inspired soft exosuit for walking assistance," *The International Journal of Robotics Research*, vol. 34, no. 6, pp. 744–762, 2015.

[9] M. Wehner, B. Quinlivan, P. M. Aubin, E. Martinez-Villalpando, M. Baumann, L. Stirling, K. Holt, R. Wood, and C. Walsh, "A lightweight soft exosuit for gait assistance," in *2013 IEEE international conference on robotics and automation*. IEEE, 2013, pp. 3362–3369.

[10] L. N. Awad, A. Esquenazi, G. E. Francisco, K. J. Nolan, and A. Jayaraman, "The rewalk restore™ soft robotic exosuit: a multi-site clinical trial of the safety, reliability, and feasibility of exosuit-augmented post-stroke gait rehabilitation," *Journal of neuroengineering and rehabilitation*, vol. 17, no. 1, pp. 1–11, 2020.

[11] S. Zabel, Z. Lockhart, N. Badiani, J. Cornish, L. Falzon, A. Flis, K. Patterson, S. Gregor, and J. Vaughan-Graham, "Physiotherapy students' perspectives on the use and implementation of exoskeletons as a rehabilitative technology in clinical settings," *Disability and Rehabilitation: Assistive Technology*, pp. 1–8, 2020.

[12] A. Schiele and F. C. Van der Helm, "Influence of attachment pressure and kinematic configuration on phri with wearable robots," *Applied Bionics and Biomechanics*, vol. 6, no. 2, pp. 157–173, 2009.

[13] J. Vaughan-Graham, D. Brooks, L. Rose, G. Nejat, J. Pons, and K. Patterson, "Exoskeleton use in post-stroke gait rehabilitation: a qualitative study of the perspectives of persons post-stroke and physiotherapists," *Journal of neuroengineering and rehabilitation*, vol. 17, no. 1, pp. 1–15, 2020.

[14] "Rewalk personal 6.0 exoskeleton for spinal cord injury." [Online]. Available: https://rewalk.com/rewalk-personal-3/

[15] C. B. Baunsgaard, U. V. Nissen, A. K. Brust, A. Frotzler, C. Ribeill, Y.-B. Kalke, N. León, B. Gómez, K. Samuelsson, W. Antepohl, *et al.*, "Gait training after spinal cord injury: safety, feasibility and gait function following 8 weeks of training with the exoskeletons from ekso bionics," *Spinal cord*, vol. 56, no. 2, pp. 106–116, 2018.

[16] P. H. Nguyen and W. Zhang, "Design and computational modeling of fabric soft pneumatic actuators for wearable assistive devices," *Scientific reports*, vol. 10, no. 1, pp. 1–13, 2020.

[17] C. Thalman and P. Artemiadis, "A review of soft wearable robots that provide active assistance: Trends, common actuation methods, fabrication, and applications," *Wearable Technologies*, vol. 1, 2020.

[18] R. V. Martinez, C. R. Fish, X. Chen, and G. M. Whitesides, "Elastomeric origami: programmable paper-elastomer composites as pneumatic actuators," *Advanced functional materials*, vol. 22, no. 7, pp. 1376–1384, 2012.

[19] T. Ranzani, S. Russo, F. Schwab, C. J. Walsh, and R. J. Wood, "Deployable stabilization mechanisms for endoscopic procedures," in *2017 IEEE International Conference on Robotics and Automation (ICRA)*. IEEE, 2017, pp. 1125–1131.

[20] S. Li, D. M. Vogt, D. Rus, and R. J. Wood, "Fluid-driven origami-inspired artificial muscles," *Proceedings of the National academy of Sciences*, vol. 114, no. 50, pp. 13 132–13 137, 2017.

[21] Z. Izadifar, X. Chen, and W. Kulyk, "Strategic design and fabrication of engineered scaffolds for articular cartilage repair," *Journal of functional biomaterials*, vol. 3, no. 4, pp. 799–838, 2012.